Journal of Catalysis **209,** 186–196 (2002)
doi:10.1006/jcat.2002.3607

Characterizations of Iron-Containing MCM-41 and Its Catalytic Properties in Epoxidation of Styrene with Hydrogen Peroxide

Ye Wang,*,[1] Qinghong Zhang,† Tetsuya Shishido,† and Katsuomi Takehira†

*State Key Laboratory for Physical Chemistry of Solid Surfaces, Department of Chemistry, Xiamen University, Xiamen 361005, China; and †Department of Applied Chemistry, Graduate School of Engineering, Hiroshima University, Kagamiyama 1-4-1, Higashi-Hiroshima 739-8527, Japan

Received December 21, 2001; revised March 12, 2002; accepted March 12, 2002

Iron-containing mesoporous molecular sieves (Fe–MCM-41) synthesized by both direct hydrothermal (DHT) and template-ion exchange (TIE) methods have been characterized and used as catalysts for the liquid-phase epoxidation of styrene with diluted H_2O_2. The characterizations with XRD, diffuse reflectance UV–vis, ESR, and EXAFS suggest that iron cations are highly dispersed and tetrahedrally coordinated with oxygen in the DHT samples with iron content lower than ca. 0.9–1.1 wt% (Si/Fe = 105–86). This coordination environment is similar to that in a ferrisilicate zeolite with MFI structure and contributes to the increase in relative strong acidic sites, as indicated by NH_3-TPD studies. On the other hand, the TIE samples mainly contain small iron oxide clusters. The conversion of styrene over the DHT catalyst increases significantly with increasing iron content up to 1.1 wt%. The selectivity to styrene oxide and the efficiency of H_2O_2 for the epoxidation can be improved by adding H_2O_2 slowly to keep the H_2O_2 concentration low during the reaction. As compared with the DHT catalyst, the TIE catalyst shows a much poorer performance for the epoxidation of styrene. It is suggested that the atomically isolated iron sites account for the epoxidation reaction with hydrogen peroxide. The iron cations incorporated inside the framework of MCM-41 do not leach during the reaction, whereas the small iron oxide clusters leach out into the liquid phase and do not contribute to the catalytic reaction.

Key Words: **iron-containing MCM-41; framework iron; epoxidation; hydrogen peroxide; styrene; leaching of active component.**

INTRODUCTION

Iron is known to be the active center in monooxygenase enzymes such as cytochrome P-450 and methane monooxygenase, which catalyze the selective oxidation of methane or several other hydrocarbons (1, 2). Many iron-containing compounds and solid catalysts have been reported to catalyze the selective oxidation of benzene or alkanes. Fenton's reagent containing Fe^{2+} and H_2O_2 is a well-known homogenous system for generating the hydroxyl radical responsible for the hydroxylation of benzene to phenol (3). An iron-containing microporous amorphous silica synthesized by a sol–gel method was reported to catalyze the conversion of benzene to phenol with H_2O_2(4). Fe–ZSM-5 catalyzed the selective oxidation of benzene to phenol with N_2O (5). Fe-containing Y zeolite modified with Pd was effective in the oxidation of alkanes such as hexane to oxygenates with a H_2O_2 or O_2–H_2 gas mixture (6). Iron phosphate catalyzed the partial oxidation of methane and ethane to their alcohols with an O_2–H_2 gas mixture (7, 8). However, to our knowledge, no iron-containing heterogeneous catalyst has been reported to show significant activity for the epoxidation of alkenes with H_2O_2, although substituted iron(III) porphyrin chlorides, typical biomimetic model complexes, are effective for epoxidation reactions with organic hydroperoxide (9).

On the other hand, metal ion-containing MCM-41, which possesses uniform nano-order mesopores and high concentrations of isolated active sites, has attracted much attention as a new type of oxidation catalyst, especially for liquid-phase oxidation reactions since facile diffusion of relatively large molecules can be expected. Many studies contributed to the syntheses and characterizations of metal ion-containing MCM-41, and some of these materials, e.g., Ti–MCM-41 and V–MCM-41, showed unique catalytic properties for the reactions of larger molecules (10–20). A few studies have been reported on the syntheses and characterizations of Fe–MCM-41 using different methods (21–23), but the details about the location and the coordination environment of iron and the amount of iron cations incorporated inside the framework of MCM-41 are still not clear. An iron-immobilized MCM-41 modified with organic silane exhibited activity in the oxidation of cyclohexane to cyclohexanol and cyclohexanone at 373 K with H_2O_2, but the leaching of active sites was unavoidable (24). The leaching of active components is a common problem in liquid-phase oxidation reactions. For example, the leaching of V and Cr was observed from V– and Cr–MCM-41, respectively, during oxidation with H_2O_2 (25). The leaching of Ti from TS-1, Ti–Alβ, Ti–MCM-41, and Ti–xerogel

[1] To whom correspondence should be addressed. Fax: (+86) 592-2183047. E-mail: yewang@jingxian.xmu.edu.cn.

0021-9517/02 $35.00

was reported in the epoxidation of crotylalcohol with H_2O_2 (26). The understanding of the nature of such leaching is vital for designing stable catalysts for liquid-phase oxidation.

It can be expected that the metal cations with different environments in mesoporous material would result in different catalytic properties and leaching behavior. Recently, we communicated that Fe–MCM-41 prepared by direct hydrothermal synthesis exhibited good performance for the epoxidation of styrene with H_2O_2 (27). In the present paper, we introduce iron into MCM-41 using two different methods, i.e., direct hydrothermal (DHT) and template-ion exchange (TIE) methods. Iron cations are added into the synthesis gel before hydrothermal synthesis in the former method, while the exchanging of Fe^{3+} in the ethanol solution with the template cations contained in the as-synthesized MCM-41 is carried out in the latter method. The synthesized materials are characterized in detail to gain insight into the coordination environments of the introduced iron cations. The influence of the environment of iron on its catalytic properties and leaching features in the epoxidation of styrene with H_2O_2 are investigated in detail.

EXPERIMENTALS AND METHODS

Synthesis

Iron was introduced into MCM-41 by two different methods. Fe–MCM-41-DHT was prepared by direct hydrothermal synthesis. Ferric nitrate, sodium silicate, and hexadecyltrimethylammonium bromide were used as the sources of iron, silicon, and template, respectively. The molar ratio of template to Si source in the synthesis gel was 0.5, which was the same as that used for the synthesis of purely silicious MCM-41. After adjustment of the pH to 10.8 with 4 N HCl, the mixture was stirred for 1 h and then transferred to a Teflon bottle placed in a stainless-steel autoclave. After hydrothermal synthesis at 423 K for 48 h, the resultant solid was recovered by filtration, thoroughly washed with deionized water (ca. 20 dm^3), dried at 313 K in a vacuum, and finally calcined in a flow of air at 823 K for 6 h. Fe–MCM-41-TIE was prepared using the template-ion exchange method, i.e., by exchanging the template cations contained in the as synthesized MCM-41 (uncalcined) with the Fe^{3+} ions in an ethanol solution. Bourlinos and coworkers (22) reported the possibility of ion exchange between the template cations and Fe^{3+} ions. In our experiment, 2 g of the as-synthesized MCM-41 comprising a ca. 50 wt% template was added to an ethanol solution of iron nitrate and stirred vigorously at 333 K for 3 h. After the ion-exchange procedure, the solid was recovered by filtration and then washed with deionized water, followed by drying at 313 K in vacuum and calcination in a flow of air at 823 K for 6 h.

Ferrisilicate with MFI structure and Fe_2O_3/Cab–O–Sil were also prepared for comparison. Ferrisilicate was prepared following the procedure of Ratnasami and Kumar (28) by hydrothermal synthesis at 443 K for 72 h using tetraethyl orthosilicate (TEOS), ferric nitrate, and tetrapropylammonium hydroxide as the silicon and iron sources and the template, respectively. The posttreatment for the as-synthesized ferrisilicate was the same as that for the Fe–MCM-41-DHT samples. XRD measurement confirmed the MFI zeolite structure. Fe_2O_3/Cab–O–Sil was prepared by a conventional impregnation method using an aqueous solution of ferric nitrate and Cab–O–Sil (M5, ACROS ORGANICS), a nonporous fumed silica with high specific surface area.

Characterization

The content of iron in each sample was determined by ICP after the sample was completely dissolved using diluted hydrochloric acid and a small amount of hydrofluoric acid. The ICP measurements were carried out using a Perkin–Elmer OPTIMA 3000.

XRD measurements were performed with a SRA M18XHF diffractometer (MAC Science Co., Ltd., Japan) with Cu $K\alpha$ radiation (40 kV, 300 mA). Small divergent and scattering slits (0.05 mm) were selected to avoid a high background at low diffraction angle.

N_2-adsorption (77 K) studies carried out with Belsorp 18SP equipment (volumetric) were used to examine the properties of mesopores of each synthesized sample. The pore size distribution was evaluated from the adsorption isotherm by the DH (Dollimore and Heal) method.

The diffuse reflectance UV–vis spectra were recorded on a Perkin–Elmer Lambda 900 UV/VIS/NIR spectrometer. The powdery sample was loaded into a quartz cell, and the spectra were collected at 200–700 nm referenced to $BaSO_4$.

ESR spectra were measured at X-band (~9 GHz) using a JEOL RE series JES-RE1X ESR spectrometer. The sample was placed in a quartz tube with an inner diameter of 3 mm and measured at ambient temperature.

X-ray absorption measurements were carried out with synchrontron radiation by using the EXAFS facilities installed at beam line BL9A of the Photon Factory, in the High Energy Accelerator Research Organization (Tsukuba, Japan), operated at 2.5 GeV with about 350–380 mA of ring current. All the data were recorded in X-ray fluorescence mode at room temperature using a Si(111) double-crystal monochromator. Ion chambers were equipped for measuring the incident beam intensity (I_0), and a lytle detector was used for measuring fluorescene yield using a Z-1 filter. Energy was calibrated with Cu K-edge absorption (8981.0 eV) and the energy resolution was 0.3 eV. The absorption was normalized to 1.0 at an energy of 30 eV higher than the absorption edge. Data analyses were performed

with the FACOM M1800 computer system at the Data Processing Center of Kyoto University (29).

NH_3-TPD measurements were carried out to obtain information about the acidic property of each catalyst using BEL JAPAN TPD-1-AT equipment. After pretreatment in a gas flow of He and O_2 at 823 K, the sample (0.2 g) was degassed in vacuum. The adsorption of NH_3 was carried out at 393 K and a pressure of 2.67 kPa for 1 h, and then the gaseous and weakly adsorbed NH_3 was purged with He. TPD was performed in He flow by raising the temperature to 873 K at a rate of 10 K min^{-1}, and the desorbed NH_3 was detected by a mass spectrometer. The fragment with $m/e = 16$ was used to quantify the amount of NH_3 desorbed because the parent peak with $m/e = 17$ was affected by the desorbed water. A known amount of NH_3 was used to calibrate the intensity of the signal with $m/e = 16$.

Catalytic Reaction

The epoxidation of alkene (styrene) was carried out using a batch-type reactor. In a typical reaction, 0.2 g of sample was added to a glass flask precharged with the desired amount of reactant and solvent at the desired temperature. The reaction was started after adding 30 wt% H_2O_2 aqueous solution. The H_2O_2 was added either all at one time at the starting point, in several batches, or continuously throughout the reaction. The reactant mixture was stirred vigorously during the reaction. After the reaction, the catalyst was filtrated and a small part of the dried catalyst was subjected to ICP measurement. All the liquid organic products were identified by GC–MS (Shimazu GCMS-QP5050) and were quantified using a gas chromatograph with a capillary column (BPX-5, 30 M × 0.25 mm) and a FID detector using toluene as an internal standard. The consumption of H_2O_2 was determined by iodometric titration.

RESULTS AND DISCUSSION

Mesoporous Structure of Materials

The porous properties obtained from N_2 adsorption measurements at 77 K are shown in Table 1. All the Fe–MCM-41 samples exhibited large surface areas of ca. 1000–1200 m^2 g^{-1} and pore volumes of ca. 0.75–1.0 ml g^{-1}. The pore distributions determined by the Dollimore and Heal (DH) method for the Fe–MCM-41 synthesized by both DHT (Si/Fe = 105) and TIE (Si/Fe = 102) methods along with the purely silicious MCM-41 are shown in Fig. 1. Narrow pore distribution around 2.5–3.0 nm was observed for all the samples.

XRD measurements showed that the diffraction lines of (100), (110), (200), and (210) at 2θ degrees of ca. 2.2, 3.6, 4.3, and 5.7° indexed to the hexagonal regularity of MCM-41 were observed for all the Fe–MCM-41 samples shown in Table 1, suggesting that the hexagonal array of mesopores in MCM-41 was sustained after the introduction of iron with both methods. The unit cell parameter (a_0), calculated from $2d(100)/\sqrt{3}$, increased with the introduction of iron into MCM-41 by the DHT method up to Fe content of ca. 0.9–1.1 wt% and remained almost unchanged or slightly decreased with a further increase in Fe content, as shown in Table 1. On the other hand, the a_0 did not change significantly on introduction of iron into MCM-41 with the TIE method. Generally, it is expected that the unit cell parameter will be enlarged after the incorporation of metal cations with ionic radius larger than Si^{4+}. Since the ionic radius of Fe^{3+} is larger than that of Si^{4+}, the increase in the a_0 may indicate that Fe^{3+} cations are incorporated into the framework of MCM-41 to replace Si^{4+} in the DHT samples. The result that the a_0 did not increase as Fe content exceeded 0.9–1.1 wt% might suggest that there existed an upper limit of iron content which could be incorporated inside the framework. That there was no significant change in the a_0

TABLE 1

Properties of Various Iron-Containing Samples

Sample[a]	Fe content in synthesis gel (wt%)	Fe content in sample by ICP (wt%)	Surface area (m^2 g^{-1})	Pore volume (ml g^{-1})	Pore diameter (nm)	a_0[b] (nm)	Color of sample	
							As synthesized	Calcined
MCM-41	0	0	1025	0.89	2.7	4.37	White	White
Fe–MCM-41-TIE (102)	0.92	0.9	1220	0.82	2.7	4.41	Brown	Brown
Fe–MCM-41-TIE (70)	1.22	1.3	1212	1.03	2.5	4.38	Brown	Brown
Fe–MCM-41-DHT (163)	0.46	0.6	1043	0.89	2.7	4.61	White	White
Fe–MCM-41-DHT (105)	0.92	0.9	1173	0.89	3.0	4.70	White	White
Fe–MCM-41-DHT (86)	1.22	1.1	1078	0.83	3.0	4.71	White	Off white
Fe–MCM-41-DHT (50)	1.82	1.8	1016	0.75	3.0	4.65	White	Off white
Ferrisilicate (MFI, 48)	1.82	1.9	350	0.38	0.55	—	White	White
Fe_2O_3/Cab–O–Sil	1.0	1.0	150	—	—	—	Brown	Brown

[a] The numbers in parentheses are the Si/Fe atomic ratios.
[b] Unit cell parameter.

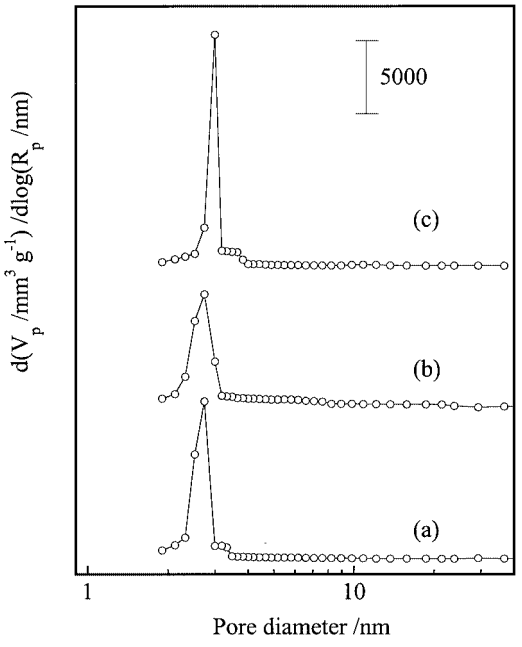

FIG. 1. Pore distributions of Fe–MCM-41. V_p and R_p in the vertical axis are pore volume and pore radius, respectively. (a) MCM-41, (b) Fe–MCM-41-TIE (Si/Fe = 102), and (c) Fe–MCM-41 DHT (Si/Fe = 105).

in the case of the TIE method suggests that no such substitution occurs or that the substitution amount is very small in the TIE samples.

Coordination Environment of Iron

The color of the Fe-containing samples synthesized in this work is also shown in Table 1 since it is a simple indication of whether bulk iron oxide exists (28). All the as-synthesized Fe–MCM-41-DHT samples exhibited a white color, suggesting that no bulk iron oxide existed and all the iron cations were probably incorporated inside the framework after hydrothermal synthesis. The white color was kept after calcination for the DHT samples with Fe content lower than 0.9 wt%. As Fe content exceeded 0.9 wt%, the calcined DHT sample became off-white in color, possibly suggesting the presence of the extraframework iron. On the other hand, the brown color of each TIE sample suggests that these samples may contain aggregated iron oxide clusters.

Figure 2 shows the diffuse reflectance UV–vis spectra. The DHT samples with iron contents of 0.9, 1.1, and 1.8 wt% exhibited a peak at ca. 265 nm (Figs. 2b–2d), which was similar to that for ferrisilicate (Fig. 2e, peak at 260 nm) containing tetrahedrally coordinated iron species. This band could be assigned to the $d\pi$–$p\pi$ charge transfer between the Fe and O atoms in the framework of Fe–O–Si in the zeolite (30). The contribution at long wavelength to this band became larger with an increase in Fe content in the DHT sample, indicating the presence of extraframework iron or aggregated Fe oxide clusters at high Fe content. These results further suggest that there exists an upper limit of iron content incorporated inside the framework of MCM-41. On the other hand, in addition to the peak at 265 nm, bands at ca. 385 and 510 nm, which were mainly observed for Fe_2O_3/Cab–O–Sil (Fig. 2h), also appeared for the TIE samples (Figs. 2f and 2g), and both bands became stronger with an increase in Fe content.

Two signals, $g = 2.0$ and 4.3, were mainly detected for the Fe-containing samples in Table 1. It was reported that the signal at $g = 4.3$ could be attributed to Fe(III) in tetrahedral coordination with strong rhombic distortion and that at $g = 2.0$ was Fe(III) in octahedral coordination (31, 32). However, such assignments seem not unambiguous, particularly for the signal at $g = 2.0$. Catana and coworkers (33) suggested that $g = 2.0$ could also be partly due to Fe(III) in a tetrahedral site although iron oxide clusters gave a large $g = 2.0$ signal. In our case (27), Fe_2O_3/Cab–O–Sil showed almost no peak at $g = 4.3$ but a strong and broad signal at $g = 2.0$. It could be considered that almost no tetrahedrally coordinated iron existed on Cab–O–Sil. The signal at $g = 4.3$ was observed for the Fe–MCM-41 prepared by the TIE method, but the relative intensity was much lower compared with that from the ferrisilicate and the Fe–MCM-41 synthesized by the DHT method. In spite of the complexity of the assignment of ESR signals, such a result still implies that iron cations are easily incorporated into the framework of MCM-41 in the DHT sample, while the number of

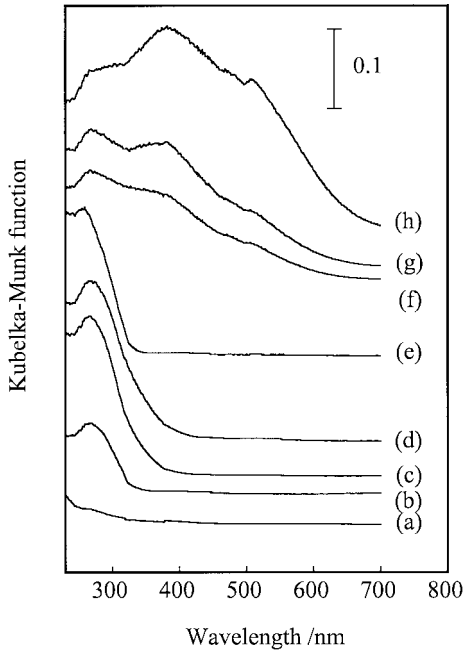

FIG. 2. Diffuse reflectance UV–vis spectra of Fe–MCM-41 along with references. (a) MCM-41, (b) Fe–MCM-41-DHT (Si/Fe = 105), (c) Fe–MCM-41-DHT (Si/Fe = 86), (d) Fe–MCM-41-DHT (Si/Fe = 50), (e) ferrisilicate (MFI, Si/Fe = 48), (f) Fe–MCM-41-TIE (Si/Fe = 102), (g) Fe–MCM-41-TIE (Si/Fe = 70), and (h) Fe_2O_3/Cab–O–Sil.

tetrahedrally coordinated iron sites in the TIE sample was very small.

It is expected that the incorporation of Fe^{3+} into the framework of MCM-41 would lead to strong Brønsted acid sites, as in the case of zeolite. Two ammonia desorption peaks at ca. 550 and 700 K were reported for the ferrisilicate with MFI structure, and these two desorptions were regarded as the weakly held ammonia, i.e., ammonia adsorbed on weak Lewis acid sites or hydrogen-bonded ones, and the strong chemisorbed ammonia or ammonium cations on the Brønsted acid sites which were related to the framework iron, respectively (34). NH_3-TPD profiles obtained over Fe–MCM-41 are shown in Fig. 3. MCM-41 without iron exhibited a main peak at ca. 500 K along with a very weak shoulder at ca. 700 K (Fig. 3a). We ascribed these minor strong acid sites to the silanol groups on defective sites (35). After introducing iron with the TIE method, both peaks were increased slightly, and there was almost no difference between the samples with Si/Fe ratios of 102 and 70 (Figs. 3b and 3c). On the other hand, the intensity of the peak at high temperature was remarkably increased by introducing iron with the DHT method (Fig. 3d). The peak at 500–520 K also became notably larger as Fe content became higher (Si/Fe = 86 (Fig. 3f) and 50 (Fig. 3g)). A similar phenomenon was observed over ferrisilicate with MFI structure, and such weak acidity was believed to arise from the extraframework iron but not the incorporated iron site (34).

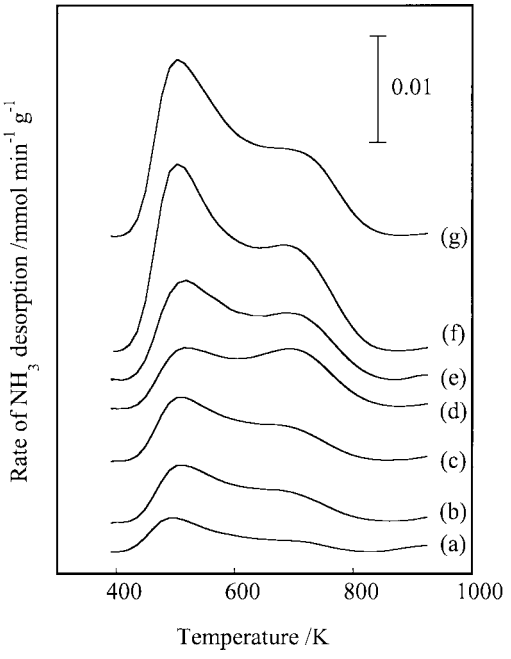

FIG. 3. NH_3-TPD profiles of Fe–MCM-41. (a) MCM-41, (b) Fe–MCM-41-TIE (Si/Fe = 102), (c) Fe–MCM-41-TIE (Si/Fe = 70), (d) Fe–MCM-41-DHT (Si/Fe = 163), (e) Fe–MCM-41-DHT (Si/Fe = 105), (f) Fe–MCM-41-DHT (Si/Fe = 86), and (g) Fe–MCM-41-DHT (Si/Fe = 50).

TABLE 2

Amount of NH_3 Desorbed from Fe–MCM-41 Synthesized by the DHT Method

Si/Fe (atomic ratio)	Fe content (wt%)	Amount of NH_3 desorbed (mmol g^{-1})		
		Peak at ca. 480–500 K	Peak at 650–700 K	Total
Purely silicious MCM-41	0	0.04	0.02	0.06
163	0.6	0.07	0.09	0.16
105	0.9	0.11	0.11	0.22
86	1.1	0.20	0.16	0.36
51	1.8	0.22	0.16	0.38
30	3.0	0.28	0.15	0.43

Table 2 summarizes the amount of NH_3 desorbed from each DHT sample. Table 2 shows that the desorption in the high-temperature region with a peak at 650–700 K increases with Fe content and remains almost unchanged as Fe content exceeds 1.1 wt% (Si/Fe = 86), whereas that in the low-temperature region with a peak at 480–500 K still increases with Fe content. If we consider that the strong acid sites are due to the iron species located in the framework, the limit amount of 0.16 mmol g^{-1} corresponds to ca. 0.9 wt% iron. Thus, the results here strongly suggest that the content of iron, which can enter the framework to replace Si^{4+}, is limited to ca. 0.9–1.1 wt%, and a further increase in Fe content will result in extraframework iron species. It should be noted that the introduction of iron with the TIE method did not lead to significant increases not only for the strong acidic sites but also for the peak of weakly adsorbed NH_3. Thus, the extraframework iron in the DHT sample may be different in chemical environment from the iron in the TIE sample.

The coordination environment of iron species has further been investigated by X-ray absorption spectroscopy, which has proven to be a powerful tool for characterizing the metal ions in molecular sieves (14). Figure 4 shows the XANES spectra of Fe–MCM-41 prepared by both TIE and DHT methods together with the reference compounds, ferrisilicate with MFI structure and α-Fe_2O_3. Iron atoms in ferrisilicate are mainly in tetrahedral coordination, whereas those in α-Fe_2O_3 are in octahedral coordination. A characteristic feature of these XANES spectra can be seen in the preedge peak at ca. 7112 eV, attributed to the so-called 1s–3d dipolar forbidden transition. Principally, this 1s–3d forbidden transition gains additional intensity when the iron center is in a noncentral symmetric environment or through mixing of 3d and 4p orbitals caused by the breakdown of inversion symmetry due to the structure distortion. Since the local symmetry around the iron is lowered from octahedral to tetrahedral coordination, the intensity (denoted as I) of this peak tends to

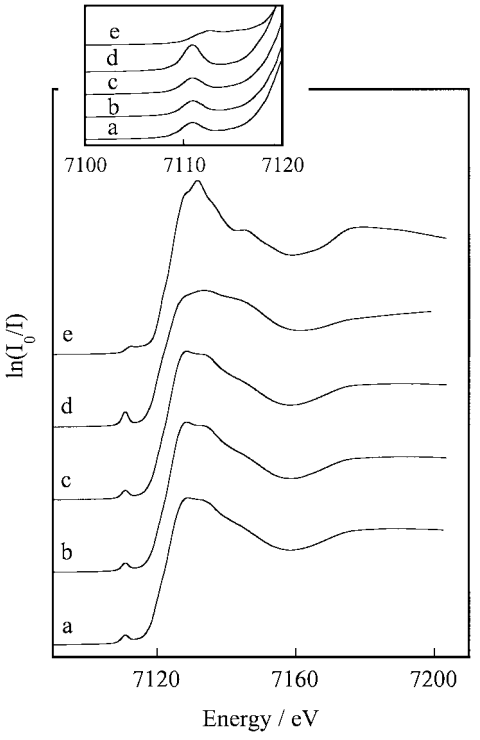

FIG. 4. Fe K-edge XANES spectra of Fe–MCM-41 along with references. (a) Fe–MCM-41-TIE (Si/Fe = 70), (b) Fe–MCM-41-DHT (Si/Fe = 163), (c) Fe–MCM-41-DHT (Si/Fe = 86), (d) ferrisilicate (MFI, Si/Fe = 48), and (e) α-Fe_2O_3.

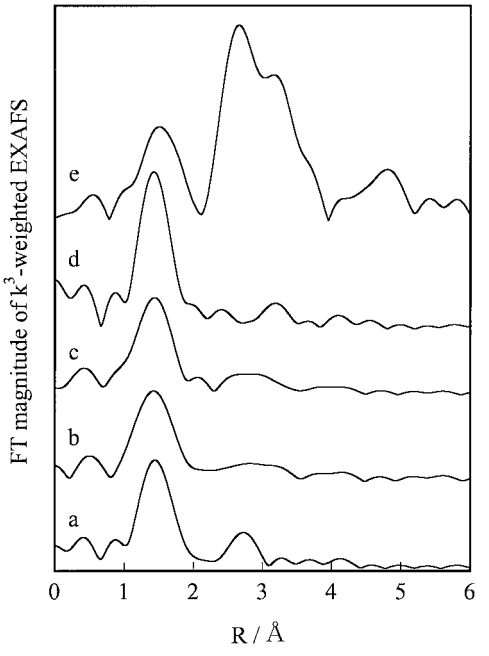

FIG. 5. Fourier transforms of k^3-weighted Fe K-edge EXAFS of (a) Fe–MCM-41-TIE (Si/Fe = 70), (b) Fe–MCM-41-DHT (Si/Fe = 163), (c) Fe–MCM-41-DHT (Si/Fe = 86), (d) ferrisilicate (Si/Fe = 48), and (e) α-Fe_2O_3.

increase, i.e., $I_{\text{tetrahedral}} > I_{\text{square pyramidal}} > I_{\text{octahedral}}$ (36). The absorption in Fig. 4 has been normalized, and thus the intensity of the preedge peak could be compared among different samples. As shown in Fig. 4, ferrisilicate which possessed a regular tetrahedral coordination structure showed the largest intensity (peak height, 0.12), whereas α-Fe_2O_3 with distorted octahedral coordination structure showed very weak absorption. The peak intensities of Fe–MCM-41-DHT samples (peak heights, 0.082 and 0.080 for Figs. 4b and 4c, respectively) were lower than that of ferrisilicate. We think that this could be explained by the difference in the framework structure of MCM-41 and that of silicalite zeolite; silicalite zeolite is crystalline, while the wall of MCM-41 is essentially amorphous. The Si–O–Fe bonds sitting in the amorphous framework of Fe–MCM41 prepared by the DHT method may thus be connected with more relaxing angles than those in ferrisilicate. Fe–MCM-41-TIE gave a smaller pre-K edge peak (peak height, 0.061) compared to the DHT samples.

Figure 5 shows the Fourier transforms of k^3-weighted Fe K-edge EXAFS spectra for Fe–MCM-41 and reference compounds. The peak at ~1.5 Å (non-phase-shift corrected) can be assigned to the contribution of the Fe–O (36). Two peaks at 2.4–3.2 Å observed for α-Fe_2O_3 (Fig. 5e) originated from two different kinds of Fe–O–Fe. The peak ascribed to Fe–O–Si also appeared around 3.0 Å (23) and can be observed as a small band for ferrisilicate (Fig. 5d). Fe–O–Fe did not exist in the Fe–MCM-41-DHT samples with Si/Fe ratios of 163 and 86 (Figs. 5b and 5c), supporting the speculation that iron dispersed as a monomer in the MCM-41, while Fe–MCM-41-TIE possessed an Fe–O–Fe bond with a length of 2.8Å (Fig. 5a, non-phase-shift corrected).

The parameters for the best fit between experimental and calculated reciprocal space spectra are given in Table 3. As for the Fe–MCM-41-DHT samples, the incorporation of the majority of Fe^{3+} into the Fe–MCM-41 framework

TABLE 3

EXAFS Data of Fe–MCM-41 Together with Reference Compounds[a]

Samples[b]	Bond	R	N	σ^2
Ferrisilicate (48)	Fe–O	1.85	3.9	−0.00071
Fe–MCM-41-DHT (163)	Fe–O	1.85	4.2	0.00173
Fe–MCM-41-DHT (83)	Fe–O	1.85	4.5	0.00250
Fe–MCM-41-TIE (70)	Fe–O	1.85	3.2	−0.00073
	Fe–O	1.99	3.2	−0.00086
	Fe–O–Fe	3.06	2.1	0.00893
α-Fe_2O_3	Fe–O	1.91	3.0	0.00070
	Fe–O	2.04	2.9	0.00230

[a] R = bond length (Å); N = coordination number; σ^2 = Debye–Waller factor (Å^2).

[b] The numbers in parentheses are the Si/Fe atomic ratios.

with a tetrahedral coordination structure can be inferred, since both the Fe–O distance (1.85 Å) and the coordination number (4.2–4.5) are closely similar to those for the ferrisilicate with MFI structure. The slightly higher coordination number of iron in the Fe–MCM-41-DHT than that in ferrisilicate may arise from the amorphous framework of MCM-41, which is not as rigid as in the case of silicalite. On the other hand, two Fe–O bonds, with lengths of 1.85 and 1.99 Å and coordination numbers of 3.2 and 3.2, respectively, were obtained in the case of Fe–MCM-41-TIE. Iron in α-Fe_2O_3 possessed two kinds of Fe–O bonds, with lengths of 1.91 and 2.04 Å and coordination numbers of 3.0 and 2.9, respectively. All these results are consistent with those obtained from UV–vis and ESR and strongly suggest that most of the iron species exist in the form of oxide clusters in the Fe–MCM-41-TIE sample. This conclusion was much different from that reported by Bourlinos and coworkers (22), who suggested that iron was incorporated into the network of MCM-41 with the TIE method. The EXAFS data in Table 3 further informed us that the coordination number of Fe–O–Fe of the Fe–MCM-41-TIE with Si/Fe ratio of 70 was 2.1, notably lower than the value (7.0) reported for α-Fe_2O_3 (37). Such a deviation might suggest that iron oxide clusters with small size exist in the channel of MCM-41.

Catalytic Properties in Epoxidation of Styrene

Styrene oxide and benzaldehyde were two main products in the epoxidation of styrene with H_2O_2 over Fe–MCM-41. Styrene glycol and benzoic acid were also formed with low selectivity, probably from the hydrolysis of styrene oxide and the consecutive oxidation of benzaldehyde, respectively, along with minor mandelic acid. Figure 6 shows the change of catalytic performances with Fe content over Fe–MCM-41 synthesized by the DHT method. The increase

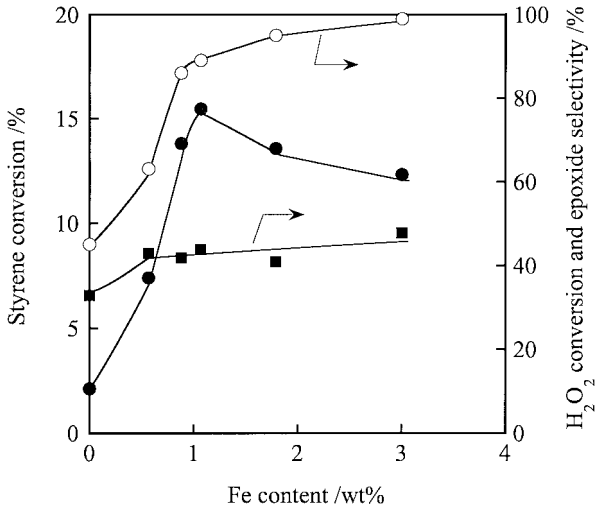

FIG. 6. Effect of Fe content on catalytic results for styrene oxidation with H_2O_2 over Fe–MCM-41-DHT. (○) H_2O_2 conversion, (●) styrene conversion, (■) styrene oxide selectivity. Conditions: $T = 346$ K; catalyst, 0.2 g; styrene, 10 mmol; H_2O_2, 9.8 mmol; DMF, 10 ml; reaction time, 2 h.

in Fe content up to 1.1 wt% increased the conversion of styrene remarkably. As Fe content exceeded 1.1 wt%, the conversion of styrene rather slightly decreased although the conversion of H_2O_2 still went up. The introduction of iron into MCM-41 raised the selectivity to styrene oxide, but the selectivity was not significantly changed with a further increase in iron content. These results indicate that an appropriate content of iron (lower than 1.1 wt%) in the DHT sample catalyzes the epoxidation of styrene, but the extra iron only enhances the decomposition of H_2O_2.

The catalytic performances of several different kinds of catalysts are compared in Table 4. Fe_2O_3/Cab–O–Sil and Fe–ZSM-5 prepared by an ion-exchange method showed medium conversion of styrene and low selectivity to styrene

TABLE 4

Comparison of Catalysts for Epoxidation of Styrene with Hydrogen Peroxide

Catalyst	Fe content (wt%)	H_2O_2 conv. (%)	Styrene conv. (%)	Selectivity (%)[a]					TOF[b] (h^{-1})
				Epoxide	Glycol	Benzald.	Benzoic acid	M. acid	
MCM-41	0	45	2.1	36.8	0	52.2	0	11.0	
Fe_2O_3/Cab–O–Sil	1.0	91	6.6	33.8	3.9	43.0	10.4	9.0	1.7
Fe–ZSM-5	0.6	95	5.0	36.9	0	63.1	0	0	4.0
Ferrisilicate	1.9	75	1.9	58.2	0	41.7	0	0	0.8
Fe–MCM-41 (TIE)	0.9	95	3.5	45.7	0	45.9	0	8.4	2.5
Fe–MCM-41 (DHT)	0.9	86	13.8	41.8	4.1	37.3	12.2	4.5	8.9
TS-1[c]			35.4	2.0		22.8			0.12
Ti–SiO_2[d]			4.5	52.5	0	47.5	0	0	6.1

Note. Reaction conditions: catalyst, 0.2 g; $T = 346$ K; styrene, 10 mmol; H_2O_2, 9.8 mmol; DMF, 10 ml; reaction time, 2 h.

[a] Benzald. and m. acid represent benzaldehyde and mandelic acid, respectively.

[b] TOF: moles of styrene oxide produced per mole of Fe or Ti in the catalyst per hour.

[c] From Ref. (38), the main product was phenylacetaldehyde (selectivity, 74.2%).

[d] From Ref. (39).

oxide, but the consumption of H_2O_2 was high. Although the selectivity to styrene oxide was high over ferrisilicate with MFI structure, the conversion of styrene was very low. Fe–MCM-41 synthesized by the TIE method also showed low conversion of styrene despite high consumption of H_2O_2, while Fe–MCM-41 synthesized by the DHT method exhibited notably high styrene conversion and moderate consumption of H_2O_2, and the highest turnover frequency for styrene oxide formation. Thus, the coordination environment of iron is crucial for the epoxidation of styrene with H_2O_2. The results shown in Table 4 and Fig. 6 combined with the characterization results described above suggest that the iron sites incorporated inside the framework of MCM-41 probably account for the epoxidation of styrene with H_2O_2, whereas the iron oxide clusters or iron species in the extraframework positions seem to accelerate the decomposition of H_2O_2. TS-1, a well-known epoxidation catalyst, gave very low selectivity to styrene oxide due to its isomerization to phenylacetaldehyde (38). A Ti–SiO_2 with highly isolated titanium cations implanted to silica synthesized by an ion-beam implantation method showed relatively high selectivity to styrene oxide, but the conversion was low (<5%) and the product shifted to benzaldehyde when the conversion was increased by increasing the temperature (39). Therefore, the iron site incorporated inside the framework of MCM-41 is very unique for epoxidation of styrene with H_2O_2.

Figure 7 shows the effect of H_2O_2 amount on the catalytic performances for the epoxidation of styrene over the Fe–MCM-41-DHT catalyst (Si/Fe = 86). In the absence of H_2O_2, very low conversion of styrene (0.13%) was observed due to the reaction with the remaining air in the reactor, and the product was only benzaldehyde. With the addition of a small amount of H_2O_2, the conversion of styrene increased sharply, and a high selectivity to styrene oxide (ca. 60%) was obtained. Although the conversion of styrene increased with an increase in the amount, or, in other words, the concentration, of H_2O_2, the selectivity to styrene oxide decreased and that to benzaldehyde and other by-products increased. More significantly, the efficiency of H_2O_2 for the epoxidation of styrene calculated by the following equation decreased drastically with an increase in H_2O_2 concentration:

$$H_2O_2 \text{ efficiency} = \frac{\text{amount of styrene oxide formed (mol)}}{\text{amount of hydrogen peroxide consumed (mol)}} \times 100(\%).$$

The efficiency of H_2O_2 was the highest (ca. 30%) at the lowest H_2O_2 concentration. Thus, in order to obtain both high conversion of styrene and high H_2O_2 efficiency, we attempted to add a certain amount of H_2O_2 (9.8 mmol) either in several batches or continuously to the reactant to keep the concentration of H_2O_2 low during the reaction. Table 5 shows the effect of the method of H_2O_2 addition on catalytic performances of the Fe–MCM-41-DHT (Si/Fe = 86). The addition of four equal batches of H_2O_2 (entry no. 2) resulted in remarkably higher selectivity to epoxide and higher H_2O_2 efficiency for epoxidation than did addition of all the H_2O_2 at the starting point. The continuous addition of H_2O_2 with a rate of 0.0735 mmol/min (entry no. 3) during the reaction further increased the selectivity to styrene oxide. The consumption of H_2O_2 was also inhibited to some extent at the same time, and thus the H_2O_2 efficiency for epoxidation increased from 7.8 to 17.4%.

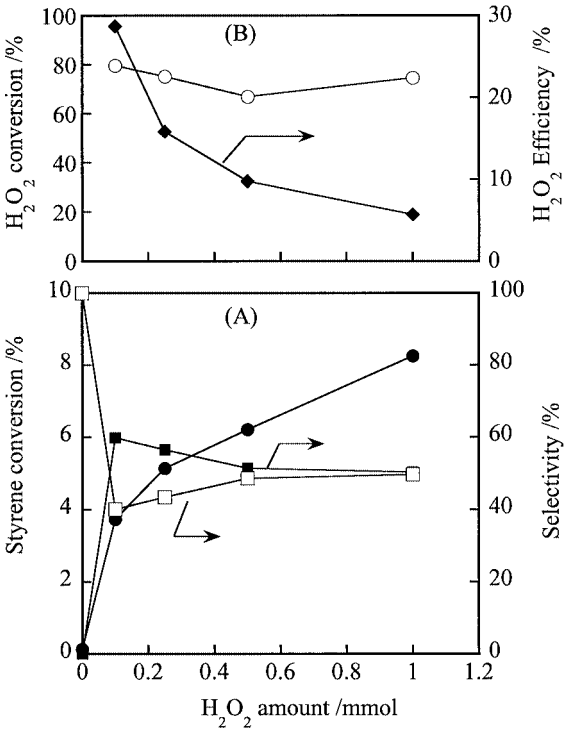

FIG. 7. Effect of H_2O_2 amount on catalytic results for styrene oxidation over Fe–MCM-41-DHT (Si/Fe = 86). (A)(●) styrene conversion, (■) styrene oxide selectivity, and (□) benzaldehyde selectivity; and (B) (○) H_2O_2 conversion and (◆) H_2O_2 efficiency for epoxidation. Conditions: T = 346 K; catalyst, 0.2 g; styrene, 10 mmol; DMF, 10 ml; reaction time, 2 h.

Figure 8 shows the change of catalytic performances with reaction time over the Fe–MCM-41-DHT (Si/Fe = 144). H_2O_2 decomposed very quickly at the initial stage and its conversion reached ca. 60% after 10 min of reaction. Styrene conversion also went up very sharply in the initial 10 min. The increase in styrene conversion continued and reached a steady state after the initial 10 min, and the consumption of H_2O_2 was very limited during this period. The selectivity to styrene oxide was almost unchanged with reaction time, and that to benzaldehyde slightly decreased along with a slight increase in that to benzoic acid. This result suggests that the epoxidation proceeds in parallel with the formation of benzaldehyde through the cleavage of the C=C bond. The consecutive oxidation of benzaldehyde gave benzoic acid.

TABLE 5

Effect of Method of H_2O_2 Addition on Catalytic Performances for Epoxidation of Styrene

Entry no.	Method of H_2O_2 addition	H_2O_2 conv. (%)	Styrene conv. (%)	Selectivity (%)[a]		TOF[a] (h^{-1})	H_2O_2 efficiency (%)
				Epoxide	Benzaldehyde		
1	Adding 9.8 mmol all at one time at the starting point	89	15.5	43.9	34.8	8.9	7.8
2	Adding 2.45 mmol every 30 min in four batches	80	17.4	59.2	37.6	13.5	13.1
3	Adding 0.98 mmol at beginning, then 0.0735 mmol/min continuously over 2 h	74	16.8	66.5	33.5	14.6	17.4

Note. Reaction conditions: catalyst Fe–MCM-41-DHT (Si/Fe = 86), 0.2 g; T = 346 K; styrene, 10 mmol; H_2O_2, 9.8 mmol; DMF, 10 ml; reaction time, 2 h.

[a] TOF: moles fo styrene oxide produced per mole of Fe in the catalyst per hour.

To get insight into the nature of the active oxygen species for the conversion of styrene, the influences of a radical scavenger, butyl hydroxy toluene (BHT), on catalytic performances over the Fe–MCM-41-DHT (Si/Fe = 86) have been investigated and the results are shown in Fig. 9. The conversion of H_2O_2 was almost unchanged after the addition of BHT up to 2 mmol but decreased from ca. 80 to 59% after the addition of 5 mmol BHT. The conversion of styrene to either styrene oxide or benzaldehyde, however, decreased drastically with an increase in the amount of BHT. Thus, the oxygen species for the formation of either styrene oxide or benzaldehyde probably possessed a radical nature. Since the selectivity to styrene oxide increased and that to benzaldehyde decreased with an increase in the amount of BHT, the oxygen species for epoxidation and that for the formation of benzaldehyde may be different.

Leaching Features of Fe–MCM-41

Table 6 shows the Fe content before and after catalytic reaction for the Fe–MCM-41 samples with different Si/Fe ratios. It is interesting that the iron content for each DHT

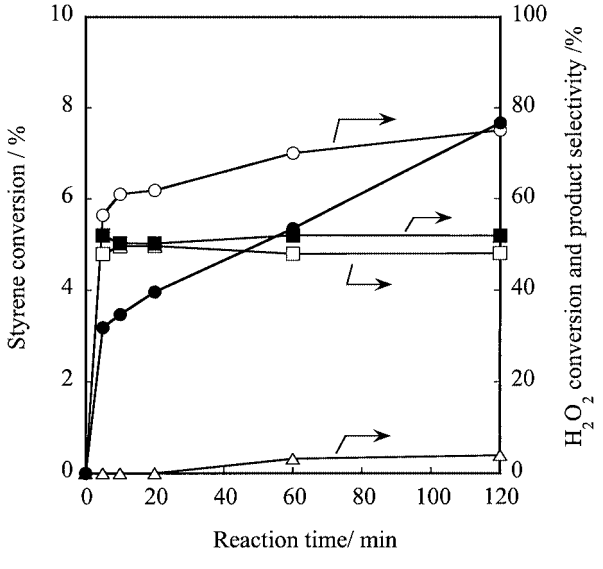

FIG. 8. Change of catalytic performances with reaction time over Fe–MCM-41-DHT (Si/Fe = 144). (○) H_2O_2 conversion, (●) styrene conversion, (■) styrene oxide selectivity, (□) benzaldehyde selectivity, and (△) benzoic acid selectivity. Conditions: T = 346 K; catalyst, 0.1 g; styrene, 10 mmol; H_2O_2, 9.8 mmol; DMF, 10 ml.

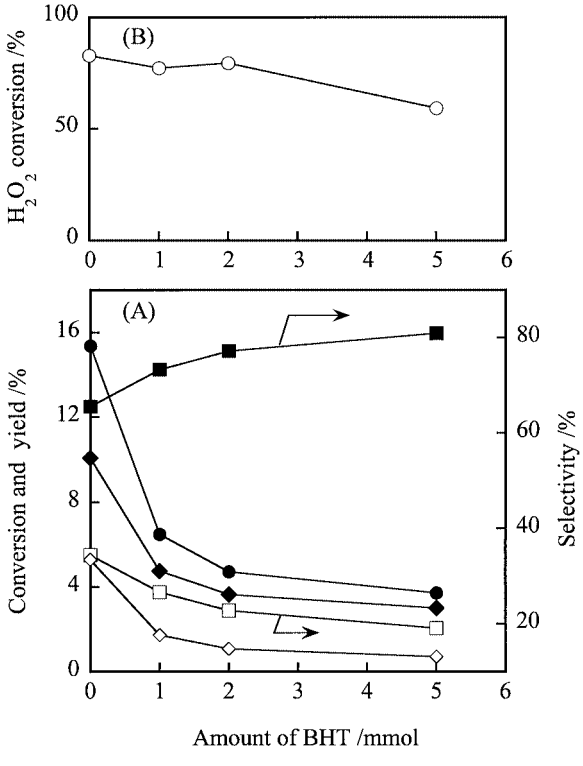

FIG. 9. Effect of a radical scavenger (BHT) on catalytic performances for styrene oxidation over Fe–MCM-41-DHT (Si/Fe = 86). (A) (●) styrene conversion, (◆) styrene oxide yield, (◇) benzaldehyde yield, (■) styrene oxide selectivity, and (□) benzaldehyde selectivity; and (B) (○) H_2O_2 conversion. Conditions: T = 346 K; catalyst, 0.2 g; styrene, 10 mmol; H_2O_2, 9.8 mmol; DMF, 10 ml.

TABLE 6

Fe Content before and after Epoxidation of Styrene with H_2O_2 over Fe–MCM-41 Catalysts

Catalyst[a]	Fe content (wt%)		Styrene conv. (%)	H_2O_2 conv. (%)	Selectivity (%)	
	Before reaction	After reaction			Epoxide	Benzaldehyde
MCM-41	0	0	2.1	45	36.8	52.2
Fe–MCM-41-DHT (163)	0.6	0.7	7.4	63	42.9	43.0
Fe–MCM-41-DHT (105)	0.9	0.8	13.8	86	41.8	37.3
Fe–MCM-41-DHT (86)	1.1	0.8	15.5	89	43.9	34.8
Fe–MCM-41-DHT (86)[b]	1.1	0.8	16.8	74	66.5	33.5
Fe–MCM-41-DHT (65)[b]	1.4	0.8	15.4	83	65.6	34.5
Fe–MCM-41-TIE (102)	0.9	0.2	3.5	95	45.7	45.9

Note. Reaction conditions: $T = 343$ K; catalyst, 0.2 g; styrene, 10 mmol; H_2O_2 (30 wt% aqueous solution), 9.8 mmol; DMF, 10 ml; reaction time, 2 h.
[a] The numbers in parentheses are the Si/Fe atomic ratios of the fresh samples.
[b] H_2O_2 (total 9.8 mmol, 1 ml) was added to the reaction mixture in four batches.

sample after reaction decreases to 0.8 wt% except for the one with iron content lower than 0.8 wt%, where no decrease in iron content occurs. In other words, the leaching of iron did not take place for the DHT sample with iron content lower than 0.8 wt%, whereas the excess iron above ca. 0.8 wt% would leach out to the liquid phase during the epoxidation of styrene with H_2O_2. On the other hand, the iron content dropped drastically from 0.9 to 0.2 wt% after the reaction for the TIE sample.

The catalytic results for the repeated use of the Fe–MCM-41-DHT (Si/Fe = 65) and the remaining iron content after each reaction cycle are shown in Table 7. The catalyst after each cycle was recovered by filtration and drying. The amount of the catalyst used for the second and third cycle decreased because of the use of a small part for ICP detection and the slight loss during the recovery. This led to some decreases in the conversions of both H_2O_2 and styrene. The selectivity to styrene oxide was almost unchanged after the first reaction cycle. The iron content decreased remarkably after the first reaction cycle, from 1.4 to 0.8 wt%. However, the activity for the second reaction cycle only decreased slightly compared with the first reaction cycle, supporting the consideration that the excess iron in the fresh catalyst did not significantly contribute to the conversion of styrene. It is interesting that the iron content after the first reaction cycle (0.8 wt%) is almost unchanged after the second and the third cycles. The results of Tables 6 and 7 indicate that the iron sites with an upper limit content of 0.8 wt% in MCM-41 introduced by the DHT method are stable toward leaching during the reaction.

The content of iron remaining after leaching was only slightly lower than the amount of iron (0.9–1.1 wt%) which existed with tetrahedral coordination with oxygen and was generally regarded to be incorporated inside the framework of MCM-41, as indicated by the characterization results. Figure 10 shows the ESR spectra of the Fe–MCM-41-DHT (Si/Fe = 65) before and after reaction. The relative strength of the signal at $g = 4.3$ which could be ascribed to the iron species with distorted tetrahedral coordination increased drastically after the first reaction cycle and almost remained constant after further reaction. This result confirms the fact that the remaining iron species, which is stable toward leaching and accounts for the epoxidation of styrene, is mainly tetrahedrally coordinated with oxygen and located in the framework of MCM-41.

TABLE 7

Repeated Uses of Fe–MCM-41 for the Epoxidation of Styrene with H_2O_2

Number of reaction cycle	Catalyst weight (g)	H_2O_2 conv. (%)	Styrene conv. (%)	Selectivity (%)		Fe content after reaction (wt%)
				Epoxide	Benzaldehyde	
						1.4
1	0.20	83	15.4	65.6	34.5	0.8
2	0.17	79	14.8	61.9	38.2	0.7
3	0.14	70	13.5	61.5	38.5	0.8

Note. Conditions: $T = 343$ K; catalyst, Fe–MCM-41-DHT (Si/Fe = 65); styrene, 10 mmol; H_2O_2, 9.8 mmol (added in four batches); DMF, 10 ml; reaction time, 2 h.

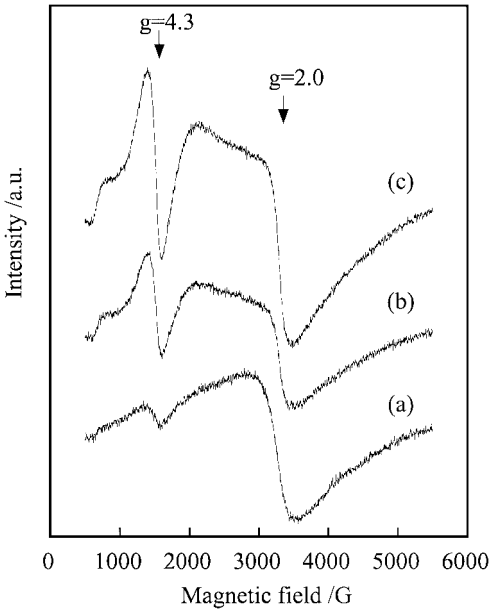

FIG. 10. ESR spectra of Fe–MCM-41-DHT (Si/Fe = 65) before and after repeated reactions. (a) Before reaction, (b) after first reaction cycle, and (c) after second reaction cycle.

CONCLUSIONS

The iron cations with an upper limit of ca. 0.9–1.1 wt% could exist in a tetrahedrally coordinated environment and probably could be incorporated inside the framework of MCM-41 in the Fe–MCM-41 prepared by direct hydrothermal synthesis. On the other hand, the exchanging of Fe^{3+} ions in the ethanolic solution with the template cations embraced in the uncalcined MCM-41 mainly resulted in small iron oxide clusters after calcination. The tetrahedrally coordinated and atomically isolated iron sites were responsible for the conversion of styrene with H_2O_2 aqueous solution. The selectivity to styrene oxide and the efficiency of H_2O_2 for epoxidation could be raised by keeping a low concentration of hydrogen peroxide during the reaction. The active oxygen species responsible for the epoxidation of styrene and for the formation of the main by-product, benzaldehyde, may be different, but it seems that both oxygen species possess a radical nature. The iron located inside the framework of MCM-41 was stable toward leaching, whereas the iron in extraframework position leached out to the liquid phase during the reaction.

REFERENCES

1. Montellano, O., "Cytochrome P-450, Structure, Mechanism and Biochemistry." Plenum, New York, 1986.
2. Rataj, M. J., Kauth, J. E., and Donnelly, M. I., *J. Biol. Chem.* **261**, 18684 (1991).
3. Fenton, H. J. H., *J. Chem. Soc.* **65**, 899 (1894).
4. Stockmann, M., Konietzni, F., Notheis, J. U., Voss, J., Keune, W., and Maier, W. F., *Appl. Catal. A* **208**, 343 (2001).
5. Panov, G. I., Uriarte, A. K., Rodkin, M. A., and Sobolev, V. I., *Catal. Today* **41**, 365 (1998).
6. Herron, N., and Tolman, C. A., *J. Am. Chem. Soc.* **109**, 2837 (1987).
7. Wang, Y., and Otsuka, K., *J. Catal.* **155**, 256 (1995), doi:10.1006/jcat.1995.1208.
8. Wang, Y., and Otsuka, K., *J. Catal.* **171**, 106 (1997), doi:10.1006/jcat.1997.1803.
9. Traylor, T. G., Kim, C., Richards, J. L., Xu, F., and Perrin, C. L., *J. Am. Chem. Soc.* **117**, 3468 (1995).
10. Sayari, A., *Chem. Mater.* **8**, 1840 (1996).
11. Corma, A., Navarro, M. T., and Perez-Pariente, J., *J. Chem. Soc. Chem. Commun.* 149 (1994).
12. Thomas, J. M., *Nature* **368**, 289 (1994).
13. Tanev, P. T., Chibwe, M., and Pinnavaia, T. J., *Nature* **368**, 321 (1994).
14. Rey, F., Sankar, G., Maschmeyer, T., Thomas, J. M., and Bell, R. G., *Top. Catal.* **3**, 121 (1996).
15. Reddy, K. M., Moudrakovski, I., and Sarari, A., *J. Chem. Soc. Chem. Commun.* 1059 (1994).
16. Morey, M., Davidson, A., Eckert, H., and Stucky, G., *Chem. Mater.* **8**, 486 (1996).
17. Luan, Z., Xu, J., He, H., Klinoswki, J., and Kevan, L., *J. Phys. Chem.* **100**, 19595 (1996).
18. Wei, D., Wang, H., Feng, X., Chueh, W.-T., Ravikovitch, P., Lyubovsky, M., Li, C., Takeguchi, T., and Haller, G. L., *J. Phys. Chem. B* **103**, 2113 (1999).
19. Yonemitsu, M., Tanaka, Y., and Iwamoto, M., *Chem. Mater.* **9**, 2679 (1997).
20. Sayari, A., Danumah, C., and Moudrakovski, I. L., *Chem. Mater.* **7**, 813 (1995).
21. Yuan, Z. Y., Liu, S. Q., Chen, T. H., Wang, J. Z., and Li, H. X., *J. Chem. Soc. Chem. Commun.* 973 (1995).
22. Bourlinos, A. B., Karakassides, M. A., and Petridis, D., *J. Phys. Chem. B* **104**, 4375 (2000).
23. Stockenhuber, M., Hudson, M. J., and Joyner, R. W., *J. Phys. Chem. B* **104**, 3370 (2000).
24. Carvalho, W. A., Wallau, M., and Schuchardt, U., *J. Mol. Catal. A* **144**, 91 (1999).
25. Carvalho, W. A., Varaldo, P. B., Wallau, M., and Schuchardt, U., *Zeolites* **18**, 408 (1997).
26. Davies, L. J., McMorn, P., Bethell, D., Page, P. C. B., King, F., Hancock, F. E., and Hutchings, G. J., *J. Catal.* **198**, 319 (2001), doi:10.1006/jcat.2000.3139.
27. Zhang, Q., Wang, Y., Itsuki, S., Shishido, T., and Takehira, K., *Chem. Lett.* 946 (2001).
28. Ratnasami, P., and Kumar, R., *Catal. Today* **9**, 329 (1991).
29. Tanaka, T., Yamashita, H., Tsuchitani, R., Funabiki, T., and Yoshida, S., *J. Chem. Soc. Faraday Trans. I* **84**, 2987 (1988).
30. Echchahed, B., Moen, A., Nicholson, D., and Bonneviot, L., *Chem. Mater.* **9**, 1716 (1997).
31. Derouane, E. G., Mestsdagh, M., and Vielvoye, L., *J. Catal.* **33**, 169 (1974).
32. Bordiga, S, Buzzoni, R., Geobaldo, F., Lamberti, C., Giamello, E., Zecchina, A., Leofanti, G., Petrini, G., Tozzola, G., and Vlaic, G., *J. Catal.* **158**, 486 (1996), doi:10.1006/jcat.1996.0048.
33. Catana, G., Pelgrims, J., and Schoonheydt, R. A., *Zeolite* **15**, 475 (1995).
34. Katada, N., Miyamoto, T., Begum, H. A., Naito, N., Niwa, M., Matsumoto, A., and Tsutsumi, K., *J. Phys. Chem. B* **104**, 5511 (2000).
35. Zhang, Q., Wang, Y., Ohishi, Y., Shishido, T., and Takehira, K., *J. Catal.* **202**, 308 (2001), doi:10.1006/jcat.2001.3276.
36. Choy, J.-H., Yoon, J.-B., Kim, D.-K., and Hwang, S.-H., *Inorg. Chem.* **34**, 6524 (1995).
37. Wong, S., Lee, J., Cheng, S., and Mou, C., *Appl. Catal. A* **198**, 115 (2000).
38. Kumar, S. B., Mirajkar, S. P., Pais, G. C. G., Kumar, P., and Kumar, R., *J. Catal.* **156**, 163 (1995), doi:10.1006/jcat.1995.1242.
39. Yang, Q., Li, C., Yuan, S., Li, J., Ying, P., Xin, Q., and Shi, W., *J. Catal.* **183**, 128 (1999), doi:10.1006/jcat.1999.2406.